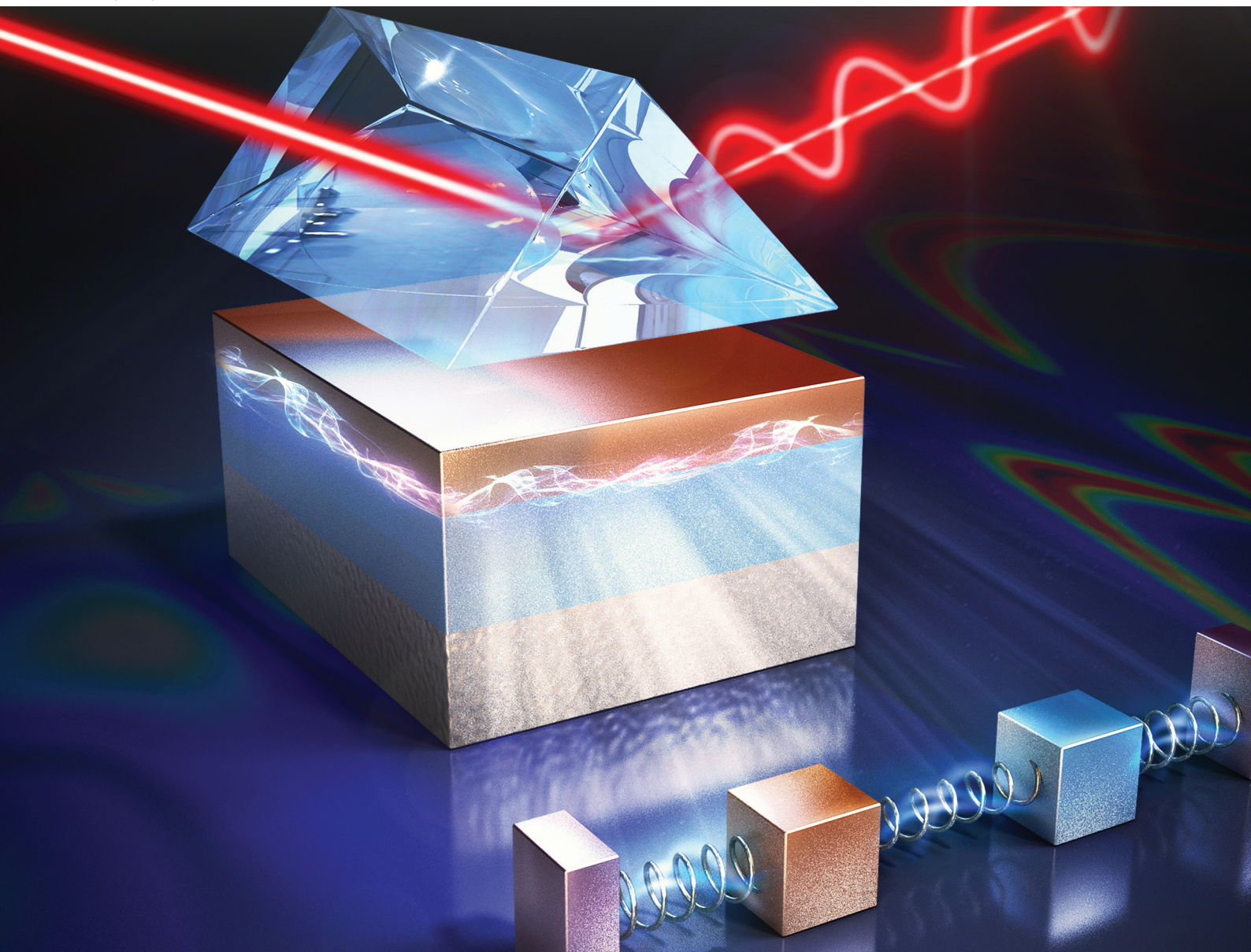


# PCCP

Physical Chemistry Chemical Physics

rsc.li/pccp



ISSN 1463-9076

**PAPER**


Gaige Zheng *et al.*

Weyl semimetal mediated epsilon-near-zero hybrid polaritons and the induced nonreciprocal radiation



Cite this: *Phys. Chem. Chem. Phys.*,  
2023, 25, 32336

# Weyl semimetal mediated epsilon-near-zero hybrid polaritons and the induced nonreciprocal radiation

Sicheng Xu,<sup>a</sup> Liming Qian,<sup>a</sup> Mengran Sun<sup>a</sup> and Gaige Zheng \*<sup>ab</sup>

Polaritonic excitation and management in ultra-thin polar crystals has recently received significant attention and holds new promise for epsilon-near-zero (ENZ) modes. However, manipulation of the ENZ mode via anisotropic magneto-optic (MO) material remains elusive. Herein, we provide an effective strategy for constructing an ENZ polar thin film with dependence on Weyl semimetals (WSM). The thermal radiation of the proposed device is explored with electromagnetic (EM) simulations that utilize the anisotropic rigorous coupled-wave analysis (aRCWA) method. Strong coupling of the ENZ mode to WSM polaritons has been demonstrated, and the structural parameters hold tolerance on the order of hundreds of nanometers, which is highly favorable for low-cost fabrication and high-performance application. By changing both the azimuthal angle ( $\phi$ ) and angle of incidence ( $\theta$ ), the nonreciprocity ( $\eta$ ) can be effectively influenced. The distribution of  $\eta$  is symmetrical with  $\phi = 180^\circ$ ,  $\eta = 0$  when  $\phi = 90^\circ$  and  $\phi = 270^\circ$ . The mechanism of this proposal is owing to the hybrid polaritons supported by the polar thin film and nonreciprocal radiation of WSM, which is validated by examining the amplitude distribution of the magnetic field. The nonreciprocal emitter described herein allows simultaneous control of spectral distribution and polarization of radiation, which will facilitate the active design and application of mid-infrared (MIR) thermal emitters.

Received 30th August 2023,  
Accepted 16th October 2023

DOI: 10.1039/d3cp04183b

rsc.li/pccp

## 1 Introduction

The hybrid light-matter nature of phonon polaritons (PhPs) in layered thin films offers a promising platform for enabling strong EM field confinement.<sup>1–5</sup> Compared to bulk crystals, the identified surface phonon polaritons (SPhPs) have recently attracted great interest due to their unique properties, which originate from the coupling of free-photons to optical phonons.<sup>6–10</sup> Recent achievements in the domain of nanophotonics have shown that SPhPs are promising constituents for MIR technology, owing to the possibility to solve the intrinsic loss challenge of plasmonics and offering great potential for technological aspects, such as all-optical switching, highly efficient sensing, or enhanced nonlinear-optical conversion efficiency.<sup>11–14</sup>

SPhPs are excitations that emerge from light-matter interaction with phonons in the strong coupling limit, yielding hybrid modes with both phononic and EM characteristics.<sup>15–18</sup>

Depending on the vibration direction with respect to the propagation direction, a contrast occurs between longitudinal optical (LO) and transverse optical (TO) modes. And the spacing between the two corresponding resonance frequencies  $\omega_{\text{TO}}$  and  $\omega_{\text{LO}}$  is expected, which is not present for non-polar crystals.<sup>19,20</sup> The Reststrahlen band (RB) where the real part of  $\epsilon_{\text{po}}$  is negative is delimited by the respective  $\omega_{\text{TO}}$  and  $\omega_{\text{LO}}$ .<sup>21</sup> The strong and controllable dispersion of the SPhPs in the RB suggests an ordinary way for changing and manipulating SPhP resonances. When different polar dielectrics are combined together to construct compound multilayers, the RBs may meet with overlapping and result in a variety of exciting effects such as strong coupling, mode-splitting, and index-sensing, thus allowing for the handling of unique hybrid polaritons with a separate polaritonic response.<sup>22–24</sup> Moreover, much more strong optical field distribution will arise for the Berreman mode in an ultrathin polar dielectric film, as the resonance wavelength locates within close range of ENZ.<sup>25–27</sup>

Stacking and combining functional materials into PhPs involved heterostructure offers a flexible and promising way to realize the active control of PhPs.<sup>28,29</sup> As an attractive material, graphene not only provides new insight into the realization of tunable dispersion via applying extra gate voltage in the MIR and terahertz frequency ranges, but also provides a

<sup>a</sup>Jiangsu Key Laboratory for Optoelectronic Detection of Atmosphere and Ocean, Nanjing University of Information Science and Technology, Nanjing, 210044, China. E-mail: jsnanophotonics@yahoo.com

<sup>b</sup>Jiangsu Collaborative Innovation Center on Atmospheric Environment and Equipment Technology, Nanjing, 210044, China

higher degree of freedom for designing.<sup>30–39</sup> In addition, phase change materials (PCMs) are also appealing as their optical properties undergo great changes under external stimuli.<sup>40–42</sup> By incorporating PCMs with polar dielectric materials, transitions of optical properties induced by a phase mutation can be used to manage polariton dispersion.

Recently, it has been found that WSM showed stronger nonreciprocity at MIR wavelengths without external magnetic fields, which results in a great enhancement in nonreciprocal thermal radiation.<sup>43–49</sup> The objective of the present work is the comprehensive characterization of the hybrid PhP modes in the Otto heterostructure including their dispersion, spectral response and field distribution. The considered system is composed of a sandwiched construction with air/aluminium nitride (AlN)/WSM/silver (Ag) and a coupling prism. In order to satisfy the excitation conditions of attenuated total reflection (ATR), the coupling prism is chosen as KRS5 with a high refractive index. Firstly, the basic structural dimensions are obtained by employing the anisotropic rigorous coupled-wave analysis (aRCWA) algorithm. The strong coupling between ENZ and polaritons in WSM has been observed. The influence of the geometrical dimensions on the nonreciprocal radiation is investigated. The effects of incidence and azimuthal angles on nonreciprocity are also tested. The field intensity distributions and spectral responses are calculated to confirm the physical origin.

## 2 Theoretical model and methods

The schematic of the proposed design is demonstrated in Fig. 1, all regions of which are denoted by numbers 1 to 4.  $\theta$

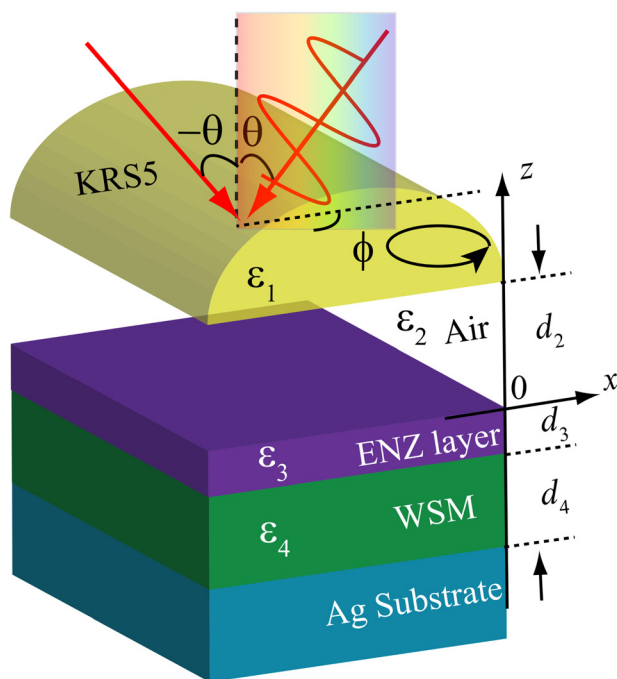


Fig. 1 Schematic of the proposed structure. All regions are denoted by numbers 1 to 4.

Table 1 Permittivity parameters for polar dielectrics

Parameter	$\epsilon_{\infty}$ (–)	$\omega_{LO}$ (cm <sup>–1</sup> )	$\omega_{TO}$ (cm <sup>–1</sup> )	$\gamma$ (cm <sup>–1</sup> )
	4.72	890	610	2.2
⊥	4.53	912	670	2.2

is the incident angle and  $\phi$  represents the azimuthal angle. In the following calculation and analysis, only the transverse magnetic (TM) mode will be investigated. The permittivity function of the polar crystal (AlN) at MIR frequencies can be described by the Lorentz oscillator model:<sup>50,51</sup>

$$\epsilon_{\text{AlN}}(\omega) = \epsilon_{\infty,||(\perp)} \frac{\omega^2 - \omega_{LO,||(\perp)}^2 - i\omega\gamma}{\omega^2 - \omega_{TO,||(\perp)}^2 - i\omega\gamma} \quad (1)$$

AlN is a uniaxial anisotropic material that can support the propagation of SPhPs, the principle dielectric permittivities differ and each of them can be defined by eqn (1) with a unique set of material parameters. AlN is an uniaxial crystal that features one extraordinary crystal axis (⊥) along which the dielectric permittivity is different from that along the two ordinary axes (||). Details of the used material parameters are summarized in Table 1.  $\epsilon_{\infty}$  is the high-frequency limit of the dielectric constant, and  $\gamma$  is the absorption relevant factor. RB is the wavelength range where the real part of dielectric permittivity  $\epsilon_{\text{po}}$  is negative, and is delimited by  $\omega_{TO}$  and  $\omega_{LO}$ .<sup>52,53</sup>

For the consistency of the symbol, the permittivity of isotropic material KRS5 and air is also denoted in the form of a tensor, as follows:

$$\overline{\overline{\epsilon}}_n = \begin{bmatrix} \epsilon_n & 0 & 0 \\ 0 & \epsilon_n & 0 \\ 0 & 0 & \epsilon_n \end{bmatrix} \quad (2)$$

$n = 1$  and  $2$ . The thickness of the air gap, ENZ thin layer and WSM layer are denoted as  $d_2$ ,  $d_3$  and  $d_4$ , respectively.

Moreover, to simplify the study process of WSM-related EM responses, we only consider the situation that the WSM hosts two Weyl nodes with opposite chirality separated by a wave vector  $2\mathbf{b}$  in momentum space. Then the permittivity tensor of WSM can be described as:<sup>48</sup>

$$\overline{\overline{\epsilon}}_W = \begin{bmatrix} \epsilon_d & 0 & j\epsilon_a \\ 0 & \epsilon_d & 0 \\ -j\epsilon_a & 0 & \epsilon_d \end{bmatrix} \quad (3)$$

where

$$\epsilon_a = \frac{be^2}{2\pi^2\hbar\omega} \quad (4)$$

We survey the diagonal term  $\epsilon_d$  based on the Kubo–Greenwood (KG) formalism, and derive the random-phase approximation

(RPA) for a two-band model with spin degeneracy:<sup>54</sup>

$$\varepsilon_d = \varepsilon_b + \frac{ir_s g_0}{6\omega} \Omega G\left(\frac{\Omega}{2}\right) - \frac{r_s g_0}{6\pi\omega} \left\{ \frac{4}{\Omega} \left[ 1 + \frac{\pi^2}{3} \left( \frac{k_B T}{E_F(T)} \right)^2 \right] + 8\Omega \int_0^{\frac{\Omega}{2}} \frac{G(\xi) - G\left(\frac{\Omega}{2}\right)}{\Omega^2 - 4\xi^2} \xi d\xi \right\} \quad (5)$$

Here,  $\varepsilon_b$  and  $E_F$  denote the background permittivity and chemical potential, respectively.  $\Omega = \hbar(\omega + i\tau^{-1})/E_F$  is the normalized complex frequency,  $\tau^{-1}$  is the Drude damping rate,  $G(E) = n(-E) - n(E)$ , where  $n(E)$  defines the Fermi distribution function,  $r_s = e^2/(4\pi\varepsilon_0\hbar\nu_F)$  is the effective fine-structure constant that determines the strength of the EM force,  $\nu_F$  is the Fermi velocity,  $g_0$  represents the number of Weyl points, and  $\xi_c = E_c/E_F$ , where  $E_c$  is the cutoff energy beyond which the band dispersion is non-linear. We will take a representative example throughout this study with the following parameters:  $T = 300$  K,  $\varepsilon_b = 6.2$ ,  $g_0 = 2$ ,  $\tau = 1000$  fs,  $\xi_c = 3$ ,  $b = 2 \times 10^9$  m<sup>-1</sup>, and  $\nu_F = 0.83 \times 10^5$  m s<sup>-1</sup>. These parameters are similar to the announced results for Co<sub>3</sub>Sn<sub>2</sub>S<sub>2</sub> and room temperature Co<sub>2</sub>MnGa.<sup>55,56</sup>

The substrate is selected as Ag, whose relative permittivity can be characterized using the Drude model:<sup>57</sup>

$$\varepsilon_{Ag}(\omega) = \varepsilon_\infty \left[ 1 - \frac{\omega_p^2}{\omega(\omega + j\Gamma)} \right] \quad (6)$$

where  $\varepsilon_\infty = 3.4$  indicates the relative permittivity of the medium at infinite frequency,  $\Gamma = 2.7 \times 10^{13}$  rad s<sup>-1</sup> is the collision frequency, and  $\omega_p = 1.39 \times 10^{16}$  rad s<sup>-1</sup> indicates the plasma frequency. Ag substrate offers a broad unity reflectivity in the MIR spectrum, thus the spectral absorptivity and emissivity can be calculated by:<sup>58</sup>

$$\begin{aligned} \alpha(\theta, \lambda) &= 1 - R(\theta, \lambda) \\ e(\theta, \lambda) &= 1 - R(-\theta, \lambda) \end{aligned} \quad (7)$$

$R(\theta, \lambda)$  and  $R(-\theta, \lambda)$  indicate the reflectivity corresponding to the incident angle of  $\theta$  and  $-\theta$ , respectively. All of the related reflectivity as well as absorptivity and emissivity are investigated through the aRCWA. The difference between  $\alpha$  and  $e$  is defined as  $\eta = |\alpha(\theta, \lambda) - e(\theta, \lambda)|$ , which is employed to measure the nonreciprocal radiation.

### 3 Strong coupling of the ENZ mode to WSM polaritons

As demonstrated in Fig. 1, the heterostructure is constituted with the top KRS5 prism with dielectric constant  $\varepsilon_1$ , the lower air gap with thickness  $d_2$  and permittivity  $\varepsilon_2$ , the ENZ layer is the AlN film with thickness  $d_3$  and permittivity  $\varepsilon_{AlN}$ , the thickness of WSM is  $d_4$ . When a TM-polarized plane wave incidences onto the structure, the EM fields take the following form in the region  $z < -d_3$ :

$$H_y = A e^{i\beta x} e^{k_4 z} \quad (8)$$

$$E_x = -iA \frac{1}{\omega \varepsilon_0 \varepsilon_4} k_4 e^{i\beta x} e^{k_4 z} \quad (9)$$

$$E_z = -A \frac{\beta}{\omega \varepsilon_0 \varepsilon_4} e^{i\beta x} e^{k_4 z} \quad (10)$$

For the fields in region  $-d_3 < z < 0$ , we have:

$$H_y = B e^{i\beta x} e^{k_3 z} + C e^{i\beta x} e^{-k_3 z} \quad (11)$$

$$E_x = -iB \frac{1}{\omega \varepsilon_0 \varepsilon_3} k_3 e^{i\beta x} e^{k_3 z} + iC \frac{1}{\omega \varepsilon_0 \varepsilon_3} k_3 e^{i\beta x} e^{-k_3 z} \quad (12)$$

$$E_z = -B \frac{\beta}{\omega \varepsilon_0 \varepsilon_3} e^{i\beta x} e^{k_3 z} - C \frac{\beta}{\omega \varepsilon_0 \varepsilon_3} e^{i\beta x} e^{-k_3 z} \quad (13)$$

For the fields in region  $0 < z < d_2$ , we have:

$$H_y = D e^{i\beta x} e^{-k_2 z} + E e^{i\beta x} e^{k_2 z} \quad (14)$$

$$E_x = iD \frac{1}{\omega \varepsilon_0 \varepsilon_2} k_2 e^{i\beta x} e^{-k_2 z} - iE \frac{1}{\omega \varepsilon_0 \varepsilon_2} k_2 e^{i\beta x} e^{k_2 z} \quad (15)$$

$$E_z = -D \frac{\beta}{\omega \varepsilon_0 \varepsilon_2} e^{i\beta x} e^{-k_2 z} - E \frac{\beta}{\omega \varepsilon_0 \varepsilon_2} e^{i\beta x} e^{k_2 z} \quad (16)$$

For the fields in region  $z > d_2$  we have:

$$H_y = F e^{i\beta x} e^{-k_1 z} \quad (17)$$

$$E_x = iF \frac{1}{\omega \varepsilon_0 \varepsilon_1} k_1 e^{i\beta x} e^{-k_1 z} \quad (18)$$

$$E_z = -F \frac{\beta}{\omega \varepsilon_0 \varepsilon_1} e^{i\beta x} e^{-k_1 z} \quad (19)$$

By employing EM boundary conditions at the interfaces with continuity of the electric field in tangential orientation and magnetic field in vertical orientation, the dispersion of the hybrid structure can be obtained as follows:

$$e^{2k_3 d_3} = \frac{Q_1 e^{2k_2 d_2} - Q_2}{Q_3 e^{2k_2 d_2} + Q_4} \quad (20)$$

$$Q_1 = \left( \frac{k_1}{\varepsilon_1} + \frac{k_2}{\varepsilon_2} \right) \left( \frac{k_2}{\varepsilon_2} - \frac{k_3}{\varepsilon_3} \right) \left( \frac{k_4}{\varepsilon_4} - \frac{k_3}{\varepsilon_3} \right) \quad (21)$$

$$Q_2 = \left( \frac{k_2}{\varepsilon_2} - \frac{k_1}{\varepsilon_1} \right) \left( \frac{k_2}{\varepsilon_2} + \frac{k_3}{\varepsilon_3} \right) \left( \frac{k_4}{\varepsilon_4} - \frac{k_3}{\varepsilon_3} \right) \quad (22)$$

$$Q_3 = \left( \frac{k_1}{\varepsilon_1} + \frac{k_2}{\varepsilon_2} \right) \left( \frac{k_2}{\varepsilon_2} + \frac{k_3}{\varepsilon_3} \right) \left( \frac{k_4}{\varepsilon_4} + \frac{k_3}{\varepsilon_3} \right) \quad (23)$$

$$Q_4 = \left( \frac{k_1}{\varepsilon_1} - \frac{k_2}{\varepsilon_2} \right) \left( \frac{k_2}{\varepsilon_2} - \frac{k_3}{\varepsilon_3} \right) \left( \frac{k_4}{\varepsilon_4} + \frac{k_3}{\varepsilon_3} \right) \quad (24)$$

$$k_n^2 = k_{ENZ}^2 - k_0^2 \varepsilon_n \quad n = 1, 2, 3, 4 \quad (25)$$

where  $k_{ENZ}$  and  $k_0$  represent the wave vectors of ENZ and air layers.  $k_n$  is the component of the wave vector perpendicular to the interface of the separate median  $n$ .

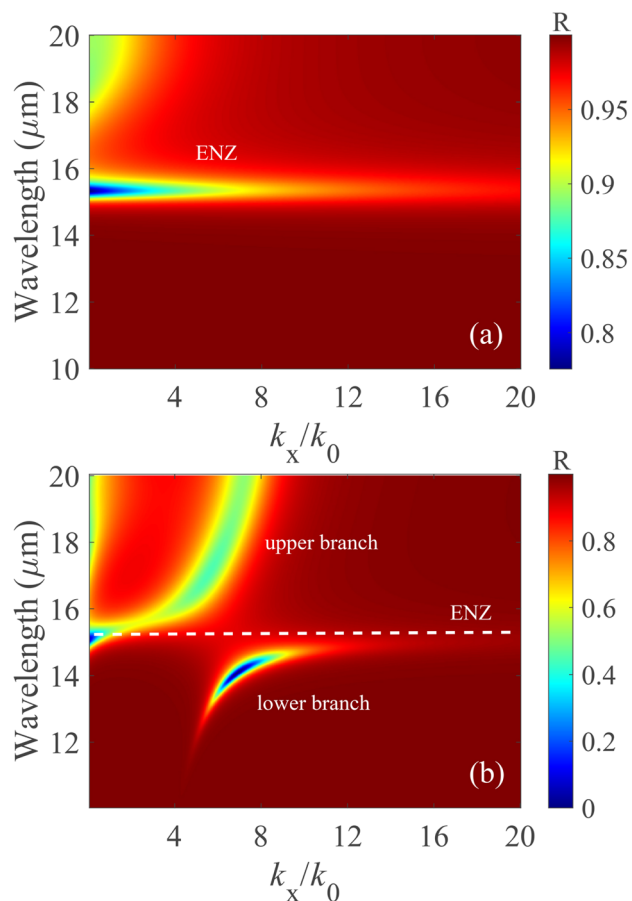


**Fig. 2** (a) Reflectivity map of the KRS5/air/AlN/Ag system, where the mode at  $\lambda_{\text{ENZ}} = 15.4 \mu\text{m}$  is considered as the ENZ mode.  $d_2 = 5 \mu\text{m}$ ,  $d_3 = 0.15 \mu\text{m}$ . (b) Reflectivity map of the KRS5/air/AlN/WSM/Ag system.  $d_2 = 5 \mu\text{m}$ ,  $d_3 = 0.15 \mu\text{m}$ ,  $d_4 = 1 \mu\text{m}$ .

For the proposed four-layer phononic system, reflectivity can be given by the Lorentzian response:<sup>59</sup>

$$R = 1 - \frac{4(\kappa_{\text{ohm}}^{\text{AlN}} + \kappa_{\text{rad}}^{\text{WSM}})\kappa_{\text{rad}}^{\text{KRS5}}}{(k_x - k_{\text{res}})^2 + (\kappa_{\text{ohm}}^{\text{AlN}} + \kappa_{\text{rad}}^{\text{WSM}} + \kappa_{\text{rad}}^{\text{KRS5}})^2} \quad (26)$$

where  $\kappa$  means spatial decay rates:  $\kappa_{\text{ohm}}^{\text{AlN}}$  represents Ohmic loss in AlN, and  $\kappa_{\text{rad}}^{\text{WSM}}$  and  $\kappa_{\text{rad}}^{\text{KRS5}}$  represent radiative leakage into WSM and KRS5, respectively. PhPs in AlN can be excited when the incident light's  $k_x$  matches with  $k_{\text{res}}$ . Zero reflectivity occurs when  $\kappa_{\text{rad}}^{\text{KRS5}} = \kappa_{\text{ohm}}^{\text{AlN}} + \kappa_{\text{rad}}^{\text{WSM}}$ , which is known as critical coupling.

We calculated the reflectivity maps of two different structures KRS5/air/AlN/Ag and KRS5/air/AlN/WSM/Ag, as shown in Fig. 2. Fig. 2(a) shows reflectivity ( $R$ ) for light incident from air onto the KRS5/air/AlN/Ag hybrid structure. The plot shows a flat dispersion

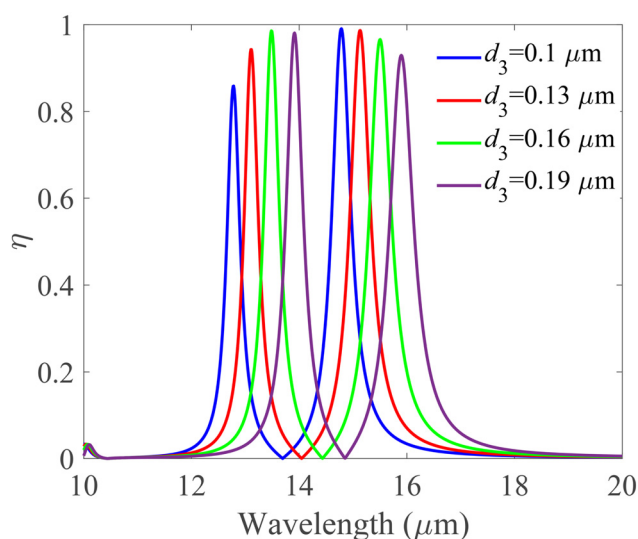


**Fig. 4**  $\eta$  spectra versus the change of  $d_3$ .  $d_2 = 5 \mu\text{m}$ ,  $d_4 = 1 \mu\text{m}$ ,  $\theta = 30^\circ$ ,  $\phi = 0^\circ$ .

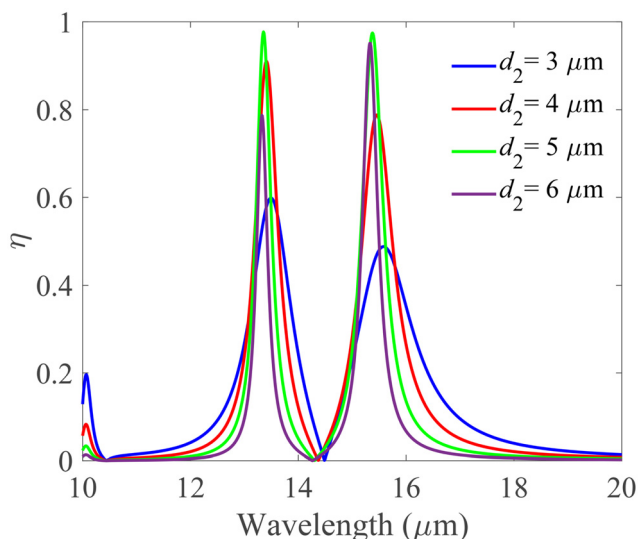


**Fig. 3**  $\eta$  spectra versus the change of  $d_2$ .  $d_3 = 0.15 \mu\text{m}$ ,  $d_4 = 1 \mu\text{m}$ ,  $\theta = 30^\circ$ ,  $\phi = 0^\circ$ .

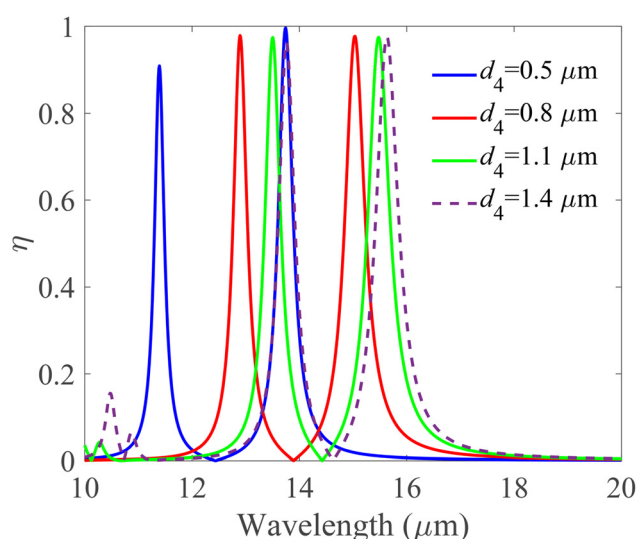


**Fig. 5**  $\eta$  spectra versus the change of  $d_4$ .  $d_2 = 5 \mu\text{m}$ ,  $d_3 = 0.15 \mu\text{m}$ ,  $\theta = 30^\circ$ ,  $\phi = 0^\circ$ .

in the vicinity of  $\lambda_{\text{ENZ}} = 15.4 \mu\text{m}$ , implying the excitation of the radiative ENZ mode. What's more important, the dispersion of WSM polaritons and the AlN ENZ mode can intersect with each other near  $\lambda_{\text{ENZ}}$ , resulting in the feasibility of strong coupling.<sup>60,61</sup> Fig. 2(b) shows  $R$  spectra of the combined WSM-ENZ mode, revealing substantially modified reflection features. An obvious anti-crossing of resonances can be found in the vicinity of  $\lambda_{\text{ENZ}}$ , related to a splitting of the total dispersion into upper and lower dual branches.

## 4 Influence of structural parameters on nonreciprocal radiation

It is well known that the Otto geometry is beneficial for an arrangement where the propagation features are not *a priori*

known, and the polariton dispersion is evaluated under critical coupling. The thickness of the air gap ( $d_2$ ) can be estimated from the condition for the constructive interference supported in the two surfaces:

$$d_2 \sqrt{\varepsilon_2} \cos \theta = \left(m + \frac{\psi_r}{2\pi}\right) \lambda \quad m = 1, 2, 3 \dots \quad (27)$$

where  $\sqrt{\varepsilon_2} = 1$  is the refractive index of air,  $\theta$  is the incidence angle, and  $\psi_r$  characterizes the phase retardation because of the reflection from the ENZ-WSM hybrid surface. Fig. 3 provides the predicted nonreciprocity curves for the KRS5/air/AlN/WSM/Ag Otto configuration with different  $d_2$  values. As can be verified from the results, when  $d_3 = 0.15 \mu\text{m}$ ,  $d_4 = 1 \mu\text{m}$ ,  $\theta = 30^\circ$  and  $\phi = 0^\circ$ , the projected  $d_2$  for critical coupling is around  $5 \mu\text{m}$ .

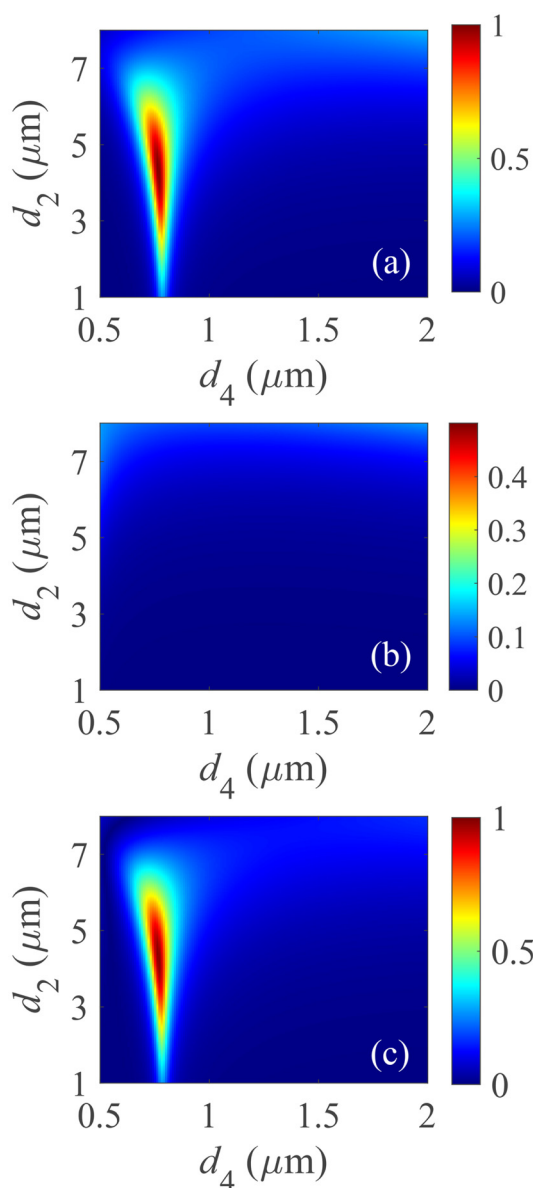


Fig. 6 (a)  $\alpha$ , (b)  $e$ , and (c)  $\eta$  varying with  $d_2$  and  $d_4$ .  $d_3 = 0.15 \mu\text{m}$ ,  $\theta = 30^\circ$ , and  $\phi = 0^\circ$ ,  $\lambda = 12.8 \mu\text{m}$ .

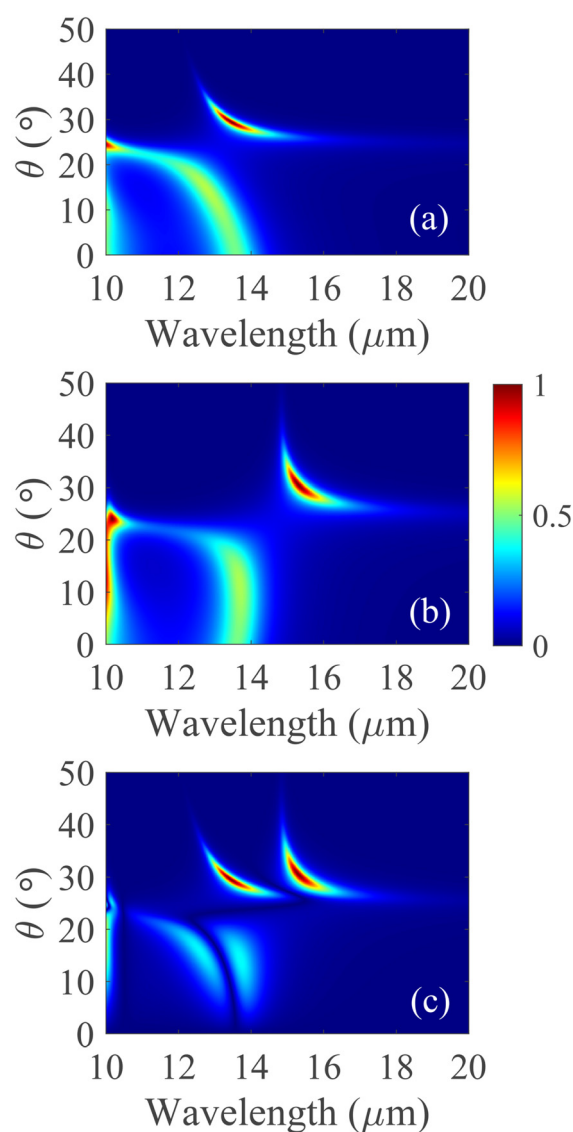


Fig. 7 Calculated absorptivity ( $\alpha$ ), emissivity ( $e$ ), and nonreciprocity ( $\eta$ ) of the structure as a function of wavelength and angle. (a)  $\alpha$ , (b)  $e$ , and (c)  $\eta$ .  $d_2 = 5 \mu\text{m}$ ,  $d_3 = 0.15 \mu\text{m}$ ,  $d_4 = 1 \mu\text{m}$ ,  $\phi = 0^\circ$ .

Ultra-thin AlN film demonstrates unique absorption resonances for TM-polarized light in the ENZ region. It has been discussed that the bounded surface modes on the upper and the lower interfaces of the film can interact with each other and lead to hybridized symmetric and antisymmetric modes.<sup>25</sup> With the further decrease of the film thickness, the symmetric mode will meet a flat dispersion band near the ENZ frequency. The AlN-WSM stacks form a dual-band nonreciprocal thermal emitter near the ENZ regions for TM-polarized light with an incidence angle of  $30^\circ$  (Fig. 4). As  $\eta$  owns a large variance with varying  $d_3$ , the nonreciprocal radiation can be controlled by altering  $d_3$ . As  $d_3$  decreases in an ENZ film, the peak of nonreciprocity spectra is red-shifted thus the optimal resonance wavelength for thin films is not always at ENZ.

At the wavelength range between  $10\ \mu\text{m}$  and  $20\ \mu\text{m}$ ,  $\eta$  spectra as a function of wavelength with changing thickness ( $d_4$ ) of WSM

is shown in Fig. 5. One can see that another peak at resonance of  $10.2\ \mu\text{m}$  appears in the spectra when  $d_4$  increases to  $1.4\ \mu\text{m}$ . With the increase of  $d_4$ , higher orders of FP resonance will be excited. However, the first order FP resonance is strong, while the other orders are weak. As shown in Fig. 5, it is clear that the non-reciprocal radiation is strong at the first order FP resonance.

The spectra of  $\alpha$ ,  $e$  and  $\eta$  as a function of  $d_2$  and  $d_4$  are shown in Fig. 6(a), (b) and (c), respectively, at a wavelength of  $12.8\ \mu\text{m}$  with an incident angle of  $30^\circ$ . The  $\alpha$  and  $e$  show large contrast, leading to perfect nonreciprocity. It is apparent that unity values of  $\alpha$  and  $\eta$  could be realized by varying  $d_2$  and  $d_4$ . Besides, it can be found that the resonance position of  $\eta$  is not much sensitive to  $d_2$  as the full width at half maxima (FWHM) of the spectra, which is consistent with the results suggested in Fig. 3. In one word, all the parameters of the design owns more than tens to hundreds of nanometers tolerance, which are beneficial and highly favourable for low-cost fabrication with high performance.

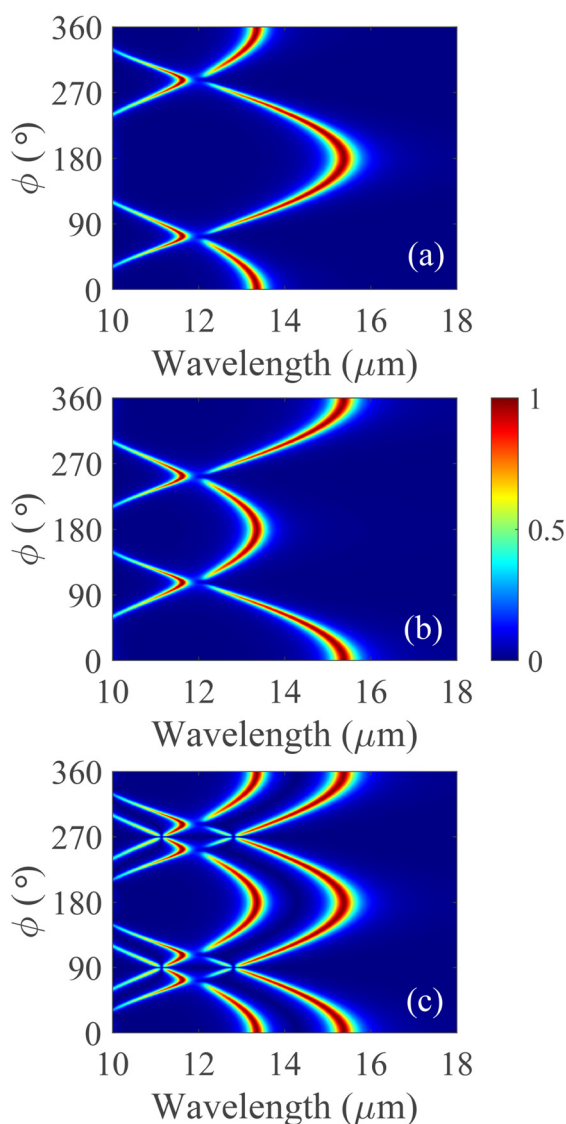


Fig. 8 (a)  $\alpha$ , (b)  $e$ , and (c)  $\eta$  varying with wavelength and the azimuthal angle  $\phi$ .  $d_2 = 5\ \mu\text{m}$ ,  $d_3 = 0.15\ \mu\text{m}$ ,  $d_4 = 1\ \mu\text{m}$ ,  $\theta = 30^\circ$ .

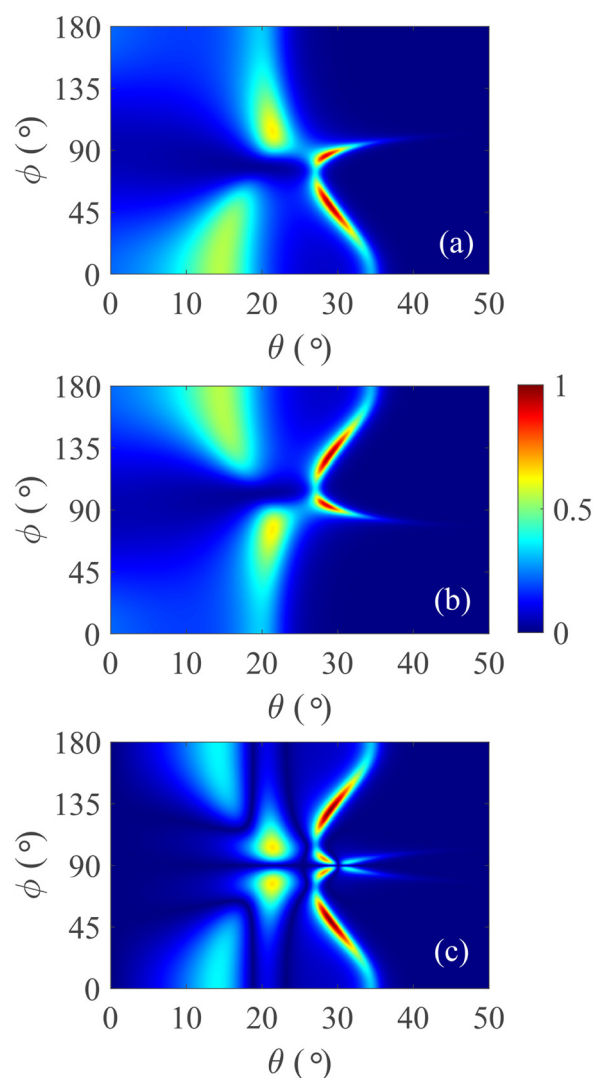


Fig. 9 The variation of (a)  $\alpha$ , (b)  $e$ , and (c)  $\eta$  with  $\theta$  and  $\phi$  when  $\lambda = 12.8\ \mu\text{m}$ . The other parameters are fixed at  $d_2 = 5\ \mu\text{m}$ ,  $d_3 = 0.15\ \mu\text{m}$ ,  $d_4 = 1\ \mu\text{m}$ .

## 5 Influence of incidence and azimuthal angles on nonreciprocal radiation

The effect of incidence angle  $\theta$  on  $\eta$  is also tested. Fig. 7 shows the angle-dependent  $\alpha$ ,  $e$  and  $\eta$  spectral maps of the proposed emitter. The parameters are chosen as  $d_2 = 5 \mu\text{m}$ ,  $d_3 = 0.15 \mu\text{m}$ ,  $d_4 = 1 \mu\text{m}$ ,  $\phi = 0^\circ$ , and TM wave incidence. From Fig. 7(a) and (b), it is evident that near-unity  $\alpha$  and  $e$  can be achieved, and the peaks don't overlap, thus two branches of near-unity  $\eta$  can be maintained under TM polarization, as shown in Fig. 7(c). Moreover, the angle dependent performance of the design suggests a feasible approach for designing nonreciprocal thermal emitters.

The azimuthal angle performs the function of an index of polarization orientation, which as a consequence could lead to modification of the peak value of  $\eta$ .<sup>62,63</sup> To explore the impact of azimuthal angle  $\phi$ , we have performed infrared nonreciprocity calculation when the TM-polarized wave is incident at a fixed angle of  $\theta = 30^\circ$ . The  $\alpha$ ,  $e$  and  $\eta$  spectra for a  $360^\circ$  rotation of  $\phi$  are given in Fig. 8(a), b and (c), respectively.

From Fig. 8(a) and (b), it is noted that the distribution of  $\alpha$  and  $e$  as functions of  $\phi$  and wavelength  $\lambda$  is symmetrical with  $\phi = 180^\circ$ . Thus when  $\phi$  falls within the range of 0 and  $2\pi$ ,  $\alpha(\phi, \lambda) = e(\pi + \phi, \lambda)$  at a determined  $\lambda$ . Fig. 8(c) confirms that  $\eta$  is

symmetric along  $\phi = 180^\circ$ . And  $\eta = 0$  when  $\phi = 90^\circ$  and  $\phi = 270^\circ$ . This is due to the fact that  $\phi$  correlates with the angle between the plane of incidence and the Weyl nodes of WSM,  $\eta = 0$  while they are perpendicular to each other. Moreover, it is obvious that multiple band strong nonreciprocity can be realized with appropriate  $\phi$ .

For a certain wavelength ( $\lambda = 12.8 \mu\text{m}$ ), we then seek to study the effects of  $\theta$  and  $\phi$  on  $\alpha$ ,  $e$  and  $\eta$ . To well propose strong nonreciprocal thermal emitters and explore the physical origin, the variation of  $\alpha$ ,  $e$  and  $\eta$  with  $\theta$  and  $\phi$  has been illustrated in Fig. 9, where  $\lambda = 12.8 \mu\text{m}$ ,  $d_2 = 5 \mu\text{m}$ ,  $d_3 = 0.15 \mu\text{m}$ ,  $d_4 = 1 \mu\text{m}$ . It is noticeable from Fig. 9(a) and (b) that both  $\alpha$  and  $e$  have double branches of near-unity intensity. Fig. 9(c) shows that  $\eta$  is symmetrical along the Azimuthal angle  $\phi = 90^\circ$ .

Fig. 10(a) shows the  $\eta$  spectra as a function of wavelength, and  $\eta$  at wavelengths of  $11.22 \mu\text{m}$ ,  $12.34 \mu\text{m}$ , and  $14.13 \mu\text{m}$ , can reach 0.802, 0.677 and 0.942, respectively. The amplitude of the incident magnetic field is considered as unity. As shown in Fig. 10(b) and (c), the magnetic fields are significantly enhanced in the ENZ and WSM layers when  $\theta = 30^\circ$ . In contrast, with  $\theta = -30^\circ$ , the  $|H_y|$  inside each layer is much weaker, implying that most of the incident energy is absorbed,  $\alpha$  is much larger than  $e$  in these two cases. In contrast, at a wavelength of  $14.13 \mu\text{m}$ , when  $\theta = -30^\circ$ ,  $|H_y|$  is greatly

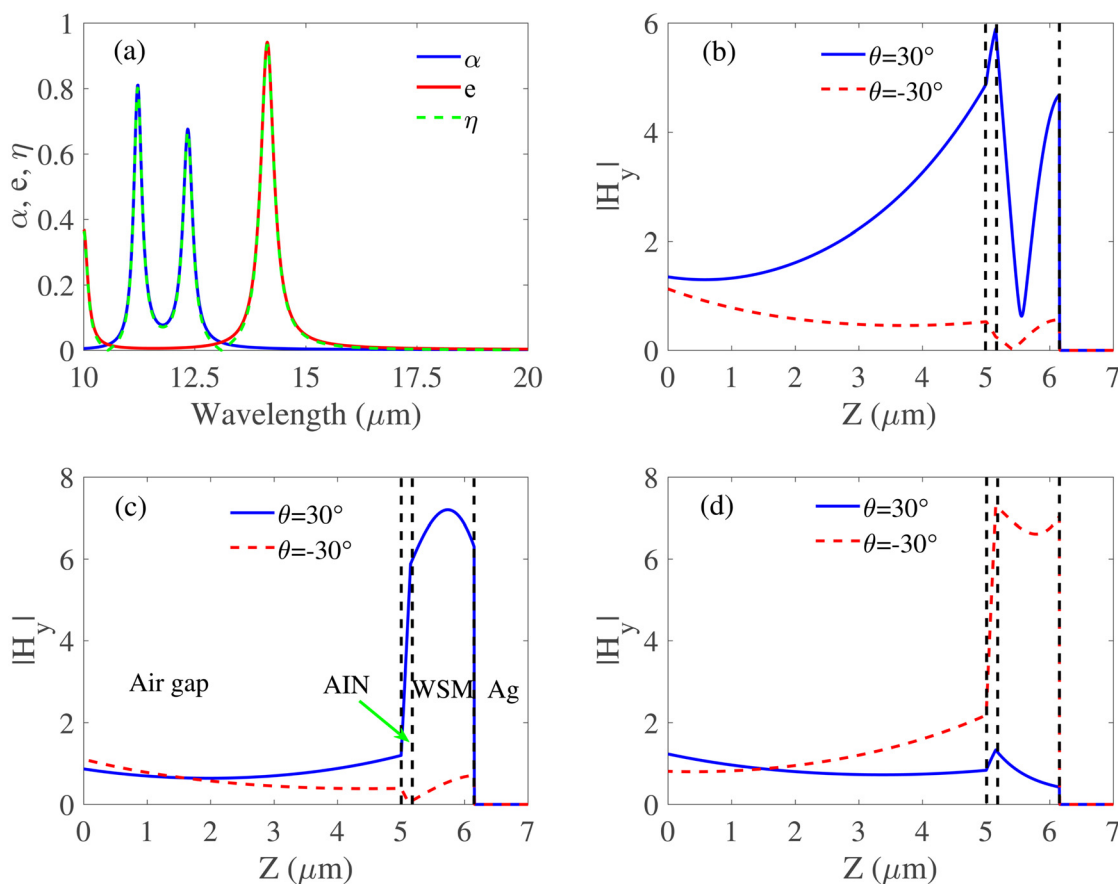


**Fig. 10** (a) Calculated absorptivity ( $\alpha$ ), emissivity ( $e$ ), and nonreciprocity ( $\eta$ ) of the structure as a function of wavelength.  $d_2 = 5 \mu\text{m}$ ,  $d_3 = 0.15 \mu\text{m}$ ,  $d_4 = 1 \mu\text{m}$ ,  $\phi = 60^\circ$ ,  $\theta = 30^\circ$ . (b) The distribution of  $|H_y|$  at a wavelength of  $11.22 \mu\text{m}$  when  $\theta$  equals  $30^\circ$  and  $-30^\circ$ . (c) The distribution of  $|H_y|$  at a wavelength of  $12.34 \mu\text{m}$  when  $\theta$  equals  $30^\circ$  and  $-30^\circ$ . (d) The distribution of  $|H_y|$  at a wavelength of  $14.13 \mu\text{m}$  when  $\theta$  equals  $30^\circ$  and  $-30^\circ$ .

enhanced in the ENZ and WSM layers, which is presented in Fig. 10(d), and  $\alpha$  is much smaller than  $e$ . In addition, the magnetic field amplitude tends to decrease as it moves away from the Ag metal under the considered wavelengths.

## 6 Summary and conclusion

In conclusion, we have studied the spectral responses in an Otto structure, which consisted of an incident medium given by a high-index KRS5 prism and an air gap, followed by AlN and WSM layers on the surface of the Ag substrate. The presented proposal enables us to study the hybrid PhP excitations at the surface of AlN–WSM layers in terms of varying Azimuthal and incident angles. We have also explicitly obtained the effect of structural parameters on the induced strong nonreciprocal radiation. We have demonstrated that the ENZ polariton supported in ultra-thin AlN layer can be used to enhance the nonreciprocal radiation. Overall, ultra-thin polar dielectric materials and the excited ENZ modes not only provide a low-loss alternative to plasmonics, but open up exciting opportunities for the manipulation of nonreciprocal radiation in the MIR region. The origin of these modes has been further analyzed by means of the  $|H_y|$ -field distribution. The hybridized modes have the characteristics of improved field confinement, which offers a novel approach to control the light–matter interaction and nonreciprocity.

## Author contributions

Sicheng Xu and Liming Qian designed the model and the computational framework and analysed the data. Mengran Sun and Gaige Zheng carried out the implementation. Sicheng Xu performed the calculations. Gaige Zheng and Sicheng Xu wrote the manuscript with input from all authors. Gaige Zheng conceived the study and was in charge of overall direction and planning.

## Conflicts of interest

There are no conflicts to declare.

## Acknowledgements

We appreciate the statistical advice and insightful comments from Prof. Yidong Hou (Sichuan University) and Jiawei Cong (Jiangsu University). This study was funded by the National Natural Science Foundation of China (Grant No. 42375127), the National Natural Science Foundation of Jiangsu Province (Grant No. BK20191396) and the Postgraduate Research and Practice Innovation Program of Jiangsu Province (Grant No. SJCX23\_0411).

## Notes and references

- 1 Z. Zheng, F. Sun, W. Huang, J. Jiang, R. Zhan, Y. Ke, H. Chen and S. Deng, *Nano Lett.*, 2020, **20**, 5301–5308.
- 2 C. R. Gubbin and S. D. Liberato, *Nanophotonics*, 2023, **12**, 2849–2864.
- 3 W. Ma, B. Shabbir, Q. Ou, Y. Dong, H. Chen, P. Li, X. Zhang, Y. Lu and Q. Bao, *InfoMat*, 2020, **2**, 777–790.
- 4 D. N. Basov, M. M. Fogler and F. J. Garcia, de Abajo, *Science*, 2016, **354**, aag1992.
- 5 J. Ordóñez-Miranda, S. Volz and M. Nomura, *Phys. Rev. Appl.*, 2021, **15**, 054068.
- 6 X. Li, G. Haberfehlner, U. Hohenester, O. Stéphan, G. Kothleitner and M. Kociak, *Science*, 2021, **371**, 1364–1367.
- 7 C. R. Gubbin, S. De Liberato and T. G. Folland, *J. Appl. Phys.*, 2022, **131**, 030901.
- 8 C. R. Gubbin and S. De Liberato, *J. Chem. Phys.*, 2022, **156**, 024111.
- 9 A. Mancini, L. Nan, F. J. Wendisch, R. Berté, H. Ren, E. Cortés and S. A. Maier, *ACS Photonics*, 2022, **9**, 3696–3704.
- 10 V. Erçağlar, H. Hajian, I. D. Rukhlenko and E. Ozbay, *Appl. Phys. Lett.*, 2022, **121**, 182201.
- 11 P. Li, X. Yang, T. Ma, Y. J. Hanss, M. Lewin, A.-K. Michel, M. Wuttig and T. Taubner, *Nat. Mater.*, 2016, **15**, 870–875.
- 12 G. Zheng, L. Xu, X. Zou and Y. Liu, *Appl. Surf. Sci.*, 2017, **396**, 711–716.
- 13 N. C. Passler, I. Razdolski, S. Gewinner, W. Schöllkopf, M. Wolf and A. Paarmann, *ACS Photonics*, 2017, **4**, 1048–1053.
- 14 U. Leon, D. Rocco, L. Carletti, M. Peccianti, S. Maci, G. Della Valle and C. De Angelis, *Sci. Rep.*, 2022, **12**, 4590.
- 15 H. Hajian, I. D. Rukhlenko, G. W. Hanson and E. Ozbay, *Photonics Nanostructures-Fundam. Appl.*, 2022, **50**, 101020.
- 16 H. Hajian, I. D. Rukhlenko, G. W. Hanson, T. Low, B. Butun and E. Ozbay, *Nanophotonics*, 2020, **9**, 3909–3920.
- 17 V. Erçağlar, H. Hajian and E. Ozbay, *J. Phys. D: Appl. Phys.*, 2021, **54**, 245101.
- 18 H. Hajian, A. Ghobadi, S. A. Dereshgi, B. Butun and E. Ozbay, *J. Opt. Soc. Am. B*, 2017, **34**, D29–D35.
- 19 C. Gubbin, R. Berte, M. Meeker, A. Giles, C. Ellis, J. Tischler, V. Wheeler, S. Maier, J. Caldwell and S. De Liberato, *Nat. Commun.*, 2019, **10**, 1682.
- 20 C. R. Gubbin and S. De Liberato, *Phys. Rev. Appl.*, 2022, **17**, 014037.
- 21 F. Cui and G. Zheng, *Opt. Mater.*, 2021, **122**, 111814.
- 22 D. C. Ratchford, C. J. Winta, I. Chatzakakis, C. T. Ellis, N. C. Passler, J. Winterstein, P. Dev, I. Razdolski, J. R. Matson, J. R. Nolen, J. G. Tischler, I. Vurgaftman, M. B. Katz, N. Nepal, M. T. Hardy, J. A. Hachtel, J.-C. Idrobo, T. L. Reinecke, A. J. Giles, D. S. Katzer, N. D. Bassim, R. M. Stroud, M. Wolf, A. Paarmann and J. D. Caldwell, *ACS Nano*, 2019, **13**, 6730–6741.
- 23 V. M. Breslin, D. C. Ratchford, A. J. Giles, A. D. Dunkelberger and J. C. Owrutsky, *Opt. Express*, 2021, **29**, 11760–11772.
- 24 W. Streyer, K. Feng, Y. Zhong, A. Hoffman and D. Wasserman, *MRS Commun.*, 2016, **6**, 1–8.

- 25 S. Campione, I. Brener and F. Marquier, *Phys. Rev. B: Condens. Matter Mater. Phys.*, 2015, **91**, 121408.
- 26 N. C. Passler, C. R. Gubbin, T. G. Folland, I. Razdolski, D. S. Katzer, D. F. Storm, M. Wolf, S. De Liberato, J. D. Caldwell and A. Paarmann, *Nano Lett.*, 2018, **18**, 4285–4292.
- 27 A. Anopchenko, S. Gurung, S. Bej and H. W. H. Lee, *Nanophotonics*, 2023, **12**, 2913–2920.
- 28 M. C. Larciprete, S. A. Dereshgi, M. Centini and K. Aydin, *Opt. Express*, 2022, **30**, 12788–12796.
- 29 S. Abedini Dereshgi, M. C. Larciprete, M. Centini, A. A. Murthy, K. Tang, J. Wu, V. P. Dravid and K. Aydin, *ACS Appl. Mater. Interfaces*, 2021, **13**, 48981–48987.
- 30 V. W. Brar, M. S. Jang, M. Sherrott, S. Kim, J. J. Lopez, L. B. Kim, M. Choi and H. Atwater, *Nano Lett.*, 2014, **14**, 3876–3880.
- 31 X. Guo, W. Lyu, T. Chen, Y. Luo, C. Wu, B. Yang, Z. Sun, F. J. García de Abajo, X. Yang and Q. Dai, *Adv. Mater.*, 2023, **35**, 2201856.
- 32 R. Fandan, J. Pedrós, J. Schiefele, A. Boscá, J. Martínez and F. Calle, *J. Phys. D: Appl. Phys.*, 2018, **51**, 204004.
- 33 Y. Hajati, Z. Zambouri and M. Sabaeian, *J. Opt. Soc. Am. B*, 2019, **36**, 1189.
- 34 A. C. Ferrari, F. Bonaccorso, V. Fal'ko, K. S. Novoselov, S. Roche, P. Bøggild, S. Borini, F. H. L. Koppens, V. Palermo, N. Pugno, J. A. Garrido, R. Sordan, A. Bianco, L. Ballerini, M. Prato, E. Lidorikis, J. Kivioja, C. Marinelli, T. Ryhänen, A. Morpurgo, J. N. Coleman, V. Nicolosi, L. Colombo, A. Fert, M. Garcia-Hernandez, A. Bachtold, G. F. Schneider, F. Guinea, C. Dekker, M. Barbone, Z. Sun, C. Galiotis, A. N. Grigorenko, G. Konstantatos, A. Kis, M. Katsnelson, L. Vandersypen, A. Loiseau, V. Morandi, D. Neumaier, E. Treossi, V. Pellegrini, M. Polini, A. Tredicucci, G. M. Williams, B. Hee Hong, J.-H. Ahn, J. Min Kim, H. Zirath, B. J. van Wees, H. van der Zant, L. Occhipinti, A. Di Matteo, I. A. Kinloch, T. Seyller, E. Quesnel, X. Feng, K. Teo, N. Rupasinghe, P. Hakonen, S. R. T. Neil, Q. Tannock, T. Löfwander and J. Kinaret, *Nanoscale*, 2015, **7**, 4598–4810.
- 35 S. Wang, F. R. Pratama, M. S. Ukhtary and R. Saito, *Phys. Rev. B*, 2020, **101**, 081414.
- 36 J. Tuček, P. Bloński, J. Ugolotti, A. K. Swain, T. Enoki and R. Zbořil, *Chem. Soc. Rev.*, 2018, **47**, 3899–3990.
- 37 S. Wang, H. Tian and M. Sun, *J. Condens. Matter Phys.*, 2023, **35**, 304002.
- 38 R. Roldán, L. Chirrolli, E. Prada, J. A. Silva-Guillén, P. San-Jose and F. Guinea, *Chem. Soc. Rev.*, 2017, **46**, 4387–4399.
- 39 H. Tian, C. Ren and S. Wang, *Nanotechnology*, 2022, **33**, 212001.
- 40 P. J. van Zwol, K. Joulain, P. Ben-Abdallah and J. Chevrier, *Phys. Rev. B*, 2011, **84**, 161413.
- 41 H. Sumikura, T. Wang, P. Li, A.-K. U. Michel, A. HeÄyler, L. Jung, M. Lewin, M. Wuttig, D. N. Chigrin and T. Taubner, *Nano Lett.*, 2019, **19**, 2549–2554.
- 42 H. Li, S. Bao and G. Zheng, *Optik*, 2021, **245**, 167720.
- 43 S. Nandy and D. A. Pesin, *Phys. Rev. B*, 2022, **106**, L041108.
- 44 C. Guo, V. S. Asadchy, B. Zhao and S. Fan, *eLight*, 2023, **3**, 2.
- 45 S. Pajovic, Y. Tsurimaki, X. Qian and G. Chen, *Phys. Rev. B*, 2020, **102**, 165417.
- 46 Y. Park, V. S. Asadchy, B. Zhao, C. Guo, J. Wang and S. Fan, *ACS Photonics*, 2021, **8**, 2417–2424.
- 47 C. Guo, B. Zhao, D. Huang and S. Fan, *ACS Photonics*, 2020, **7**, 3257–3263.
- 48 B. Zhao, C. Guo, C. A. C. Garcia, P. Narang and S. Fan, *Nano Lett.*, 2020, **20**, 1923–1927.
- 49 H. Li and G. Zheng, *Int. J. Heat Mass Transfer*, 2024, **218**, 124737.
- 50 J. D. Caldwell, L. Lindsay, V. Giannini, I. Vurgaftman, T. L. Reinecke, S. A. Maier and O. J. Glembocki, *Nanophotonics*, 2015, **4**, 44–68.
- 51 C. R. Gubbin and S. De Liberato, *Phys. Rev. X*, 2020, **10**, 021027.
- 52 L. Y. Beliaev, E. Shkondin, A. V. Lavrinenko and O. Takayama, *J. Vac. Sci. Technol. A*, 2021, **39**, 043408.
- 53 N. C. Passler, C. R. Gubbin, T. G. Folland, I. Razdolski, D. S. Katzer, D. F. Storm, M. Wolf, S. De Liberato, J. D. Caldwell and A. Paarmann, *Nano Lett.*, 2018, **18**, 4285–4292.
- 54 M. Sun, L. Qian, J. Ye, F. Xian and G. Zheng, *IEEE Photonics Tech. Lett.*, 2023, **35**, 545–548.
- 55 Q. Wang, Y. Xu, R. Lou, Z. Liu, M. Li, Y. Huang, D. Shen, H. Weng, S. Wang and H. Lei, *Nat. Commun.*, 2018, **9**, 3681.
- 56 X. Han, A. Markou, J. Stensberg, Y. Sun, C. Felser and L. Wu, *Phys. Rev. B*, 2022, **105**, 174406.
- 57 X. Wu and C. Fu, *AIP Adv.*, 2017, **7**, 075208.
- 58 Z. M. Zhang, X. Wu and C. Fu, *J. Quantum Spectrosc. Radiat. Transfer*, 2020, **245**, 106904.
- 59 B. Neuner, D. Korobkin, C. Fietz, D. Carole, G. Ferro and G. Shvets, *Opt. Lett.*, 2009, **34**, 2667–2669.
- 60 J. Wu, H. Li, C. Fu and X. Wu, *Int. J. Therm. Sci.*, 2023, **184**, 107902.
- 61 H. Xu, M. Yang and Y. Chen, *J. Phys. Chem. C*, 2022, **126**, 4024–4029.
- 62 J. Wu, B. Wu, K. Shi, X. Wu and C. Fu, *Int. J. Therm. Sci.*, 2023, **187**, 108172.
- 63 X. Wu, C. A. McEleney, Z. Shi, M. González-Jiménez and R. Macêdo, *ACS Photonics*, 2022, **9**, 2774–2782.